Observation of Fatigue Crack Propagation Mode Transition under Cyclic Torsion Using Micro-CT Imaging with Ultra-Bright Synchrotron Radiation

Y. Nakai[1], D. Shiozawa[1], T. Murakami[1], and H. Nosho[1]

[1] Department of Mechanical Engineering, Kobe University

nakai@mech.kobe-u.ac.jp

Abstract. *In the present study, micro computed tomography imaging by using ultra-bright synchrotron radiation X-ray (SR μCT), which was generated at SPring-8, was applied to the observation of torsion fatigue crack propagation behavior. It is well known that the transition of crack propagation from the shear mode to the tensile mode takes place under torsion fatigue of round bar. The transition condition, however, has not been discussed in detail since the crack growth behavior under the surface cannot be provided precisely by the conventional techniques, such as optical microscope, scanning electron microscope, and atomic force microscope. A compact torsion fatigue-testing machine was developed to conduct fatigue tests and measurements of SR μCT concurrently at Spring-8. The shape of torsion fatigue cracks could be evaluated quantitatively and nondestructively, and the transition of crack propagation from the shear mode to the tensile mode could be observed three dimensionally. The condition of the transition of crack propagation was discussed by considering the three-dimensional shape of cracks.*

INTRODUCTION

Since most of machine components are operated under combined cyclic stress state, the behavior of fatigue cracks under the mixed mode loading has been studied [1],[2]. One of the most typical mixed mode crack propagation behavior arises under cyclic torsion, where the crack propagation behavior is complex. First it propagates by the shear mode, then propagation changes to the tensile mode. The crack propagation behavior during fatigue has been studied through the observation of cracks at the surface either by direct or indirect method. However, it is not always easy to discuss the behavior of cracks by the conventional techniques, such as the replication technique, those provide us only the information at the surface. Therefore, the transition condition for the shear mode to the tensile mode for crack propagation could not be discussed in detail.

The authors have been applied the micro computed-tomography (μCT) with the ultra-bright synchrotron radiation to the three-dimensional measurement of inclusions

and cracks in fretting fatigue cracks and corrosion pit in environmental fatigue [3]-[7], and the structures and shapes of cracks inside the material were successfully observed.

In the present study, the behavior of fatigue cracks under the cyclic torsion from the initiation to the unstable fracture was observed, and the condition of the transition for crack propagation from shear to tensile mode was quantitatively discussed by considering three-dimensional shape of cracks which was obtained by the μCT. A compact torsion fatigue testing machine was developed to conduct fatigue tests at the ultra-bright synchrotron radiation facility, SPring-8.

MATERIAL AND EXPERIMENTAL PROCEDURE

Material and specimen

The material for this study was a titanium alloy, (JIS Ti-6Al-4V). The chemical composition of the titanium alloy was as follows: 0.01C, 3.96V, 6.23Al, 0.14O, 0.01N, 0.15Fe, and balance Ti (in mass%). The 0.2 % proof stress was 868 MPa, the tensile strength was 995 MPa, and the elongation was 18 %. The shape and dimensions of the specimen are shown in Figure 1. The microstructure of Ti-6Al-4V used in the present study is presented in Figure 2, that is equiaxial and the average grain size was 8 μm.

Torsion fatigue-testing machine

To clarify the fatigue crack propagation behavior, series of CT imaging should be conducted for the same crack. Then fatigue test should be conducted at the synchrotron radiation facility. For this purpose, a compact torsion fatigue test machine was developed, which is shown in Figure 3. The dimension and mass of the machine are approximately 500 mm × 200 mm × 200 mm, and 10kg respectively. The torque was applied by a direct drive motor, whose capacity was 5.0 Nm. The rotary type motor directly transfers the torque to the specimen, so that the fatigue-testing machine did not require load transfer mechanism, then downsizing of machine and high precision control of torque could be conducted. In the present experiments, fully reversed cyclic

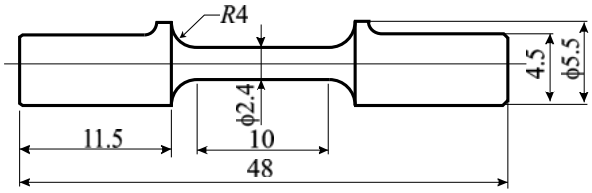

Figure 1. Shape and dimensions of specimen (in mm).

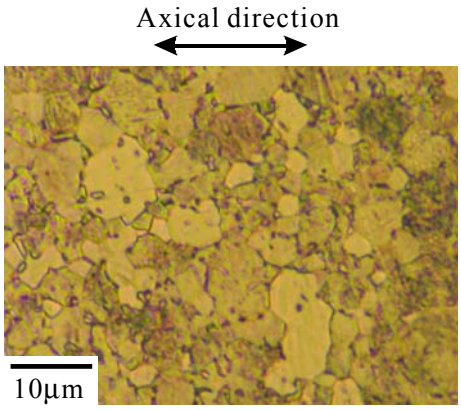

Figure 2. Microstructure of material.

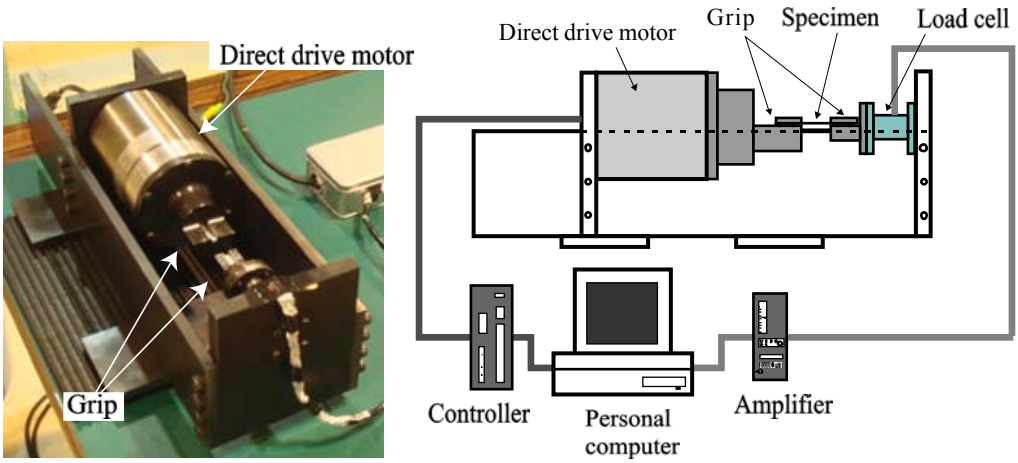

Figure 3. Torsion fatiue testing machine.

torsion (R= −1) with a frequency of 10 Hz was applied to the specimen. The fatigue-testing machine was set nearby the experimental hatch of a beam line of Spring-8.

CT imaging

X-ray imaging was carried out at BL19B2 beam line of SPring-8, which is the brightest synchrotron radiation facility in Japan. X-ray energy was adjusted to 35 keV with silicon double-crystal monochromator. The distance between a bending magnet (X-ray source) and the specimen was about 100 m. The projection image of penetrated X-ray was observed by an X-ray area detector. The detector was composed of a beam monitor (Hamamatsu Photonics AA50) and cooled CCD camera (Hamamatsu Photonics C4880 41S). Transmitted X-ray was converted to visible light through a thin phosphor screen and projected to the CCD camera by an optical relay-lens. Series of projection images of the specimen were obtained every 0.3° from 0° to 180° by rotating the specimen. To utilize the phase contrast effect, the X-ray area detector was set by 0.7 m behind the sample. Slice images were reconstructed from the series of projection images by filtered-back projection algorithm. It provided a 3D image with a grayscale color map that was proportional to the local X-ray attenuation coefficient.

EXPERIMENTAL RESULTS AND DISCUSSION

The successive observation of fatigue crack propagation behavior could be conducted by using the newly developed fatigue-testing machine and SR μCT imaging. Figures 4 and 5 show the CT images of the crack (Crack A), which initiated fatigue test under shear stress amplitude, τ_a, of 450 MPa. These images indicate the map of X-ray attenuation coefficient. Cracks were emerged by black line or, white and black lines due to the phase contrast because it generates distinct white and black lines at the

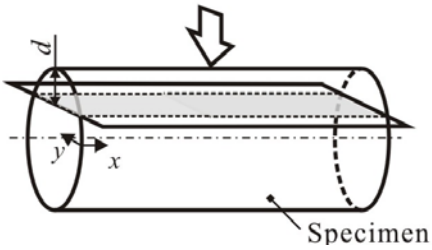

(a) Schematic description of cross sectional images

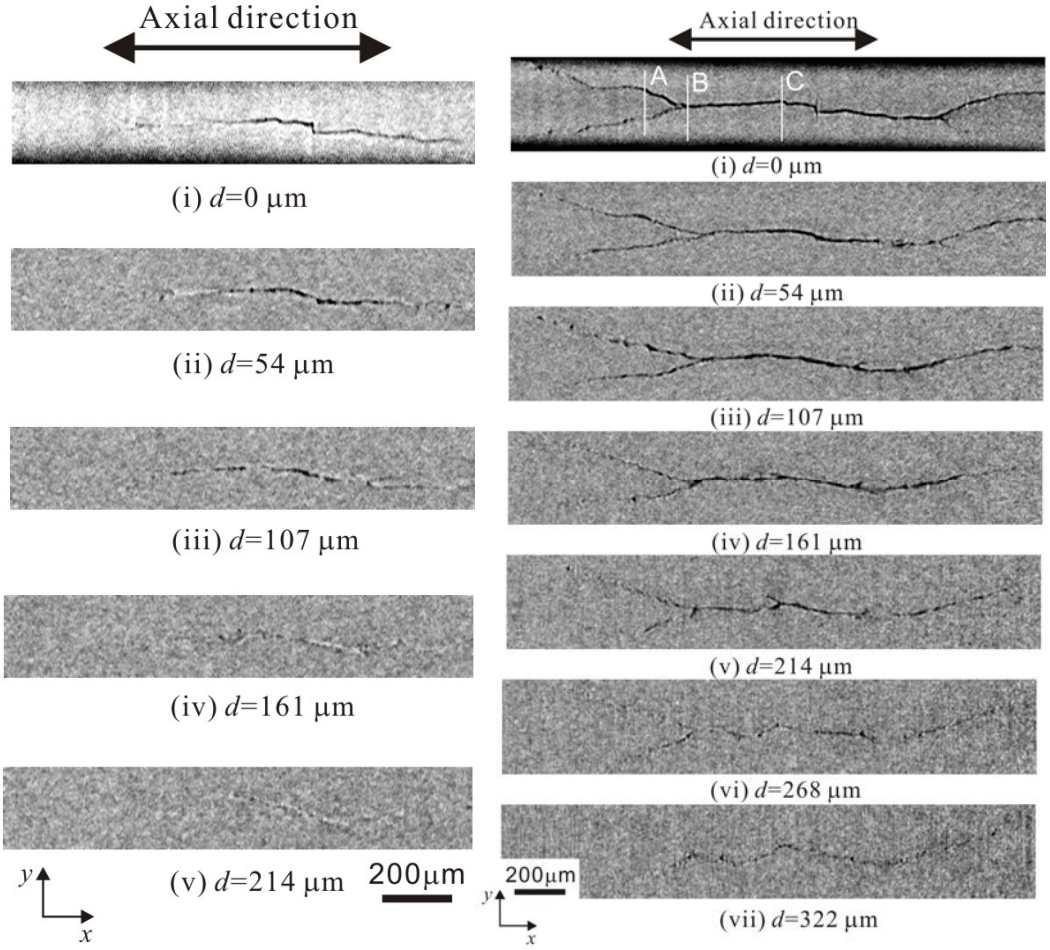

(b) Section images at N=1.62×10^5 cycles

(c) Section images at N=1.84×10^5 cycles

Figure 4. CT image of Crack A under τ_a=450 MPa.

interface of dissimilar materials and the phase contrast emphasized the crack whose opening distance was small. Figure 6 is an example of a 3D image of a crack which was initiated at a stress amplitude, τ_a, of 450MPa and N=1.86×10^5 cycles. 3D image was constructed by binalizing the X-ray attenuation coefficient map. These figures show that the shape and dimensions of torsion fatigue cracks could be evaluated quantitatively and nondestructively by SR μCT imaging.

Crack initiated and propagated in the direction parallel to the specimen axis by the shear mode (Figure 4 (b)). At N=1.84×10^5 cycles, the crack branched at the surface (Figure 4(c)).

The CT images, shown in Figure 4, were not enough contrast to determine the site of crack tips automatically by using image processing software, those were determined manually. Figure 7 shows shapes and dimensions of the cracks obtained from the μCT images, where solid marks indicate the position of crack tips before the branching, and open marks indicate those after the branching.

Before 1.53×10^5 cycles, very shallow crack was formed, and then the crack grew in the depth direction from 1.53×10^5 cycles to 1.64×10^5 cycles without accompanying the growth at the surface. This kind of non-propagation of Mode II crack was related to the crack tip shielding [8],[9]. The branching of crack took place when the crack depth

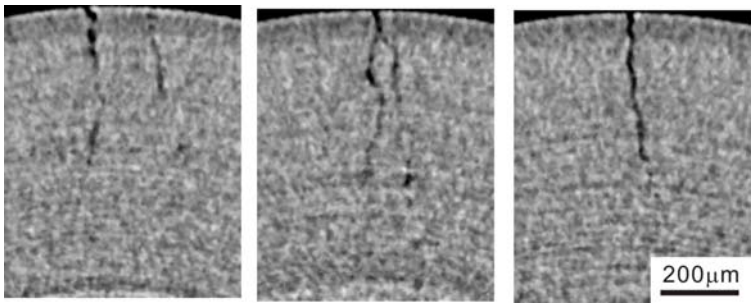

(a) A in Figure 4 (b) B in Figure 4 (c) C in Figure 4

Figure 5. Crosssection image of crack shown in Figure 4 (N=1.84×10^5 cycles).

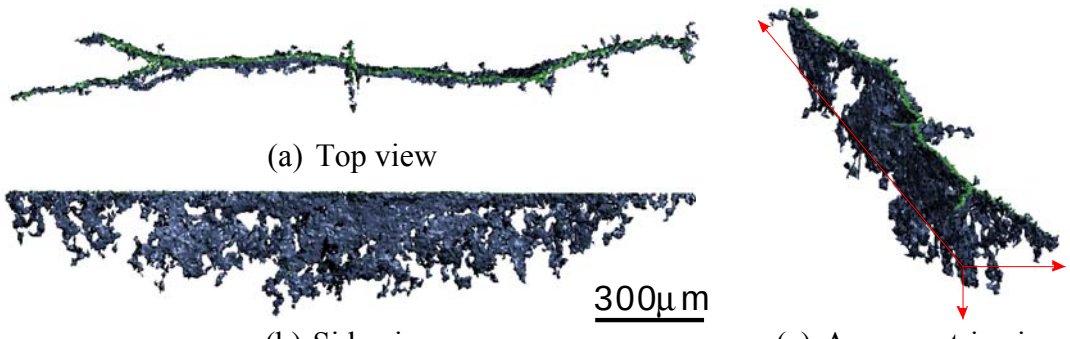

(a) Top view

(b) Side view

(c) Axonometric view

Figure 6 CT image of a crack initiated in cyclic torsion (Same crack as Figures 4 and 5). (τ_a=450 MPa, N = 1.86x10^5 cycles)

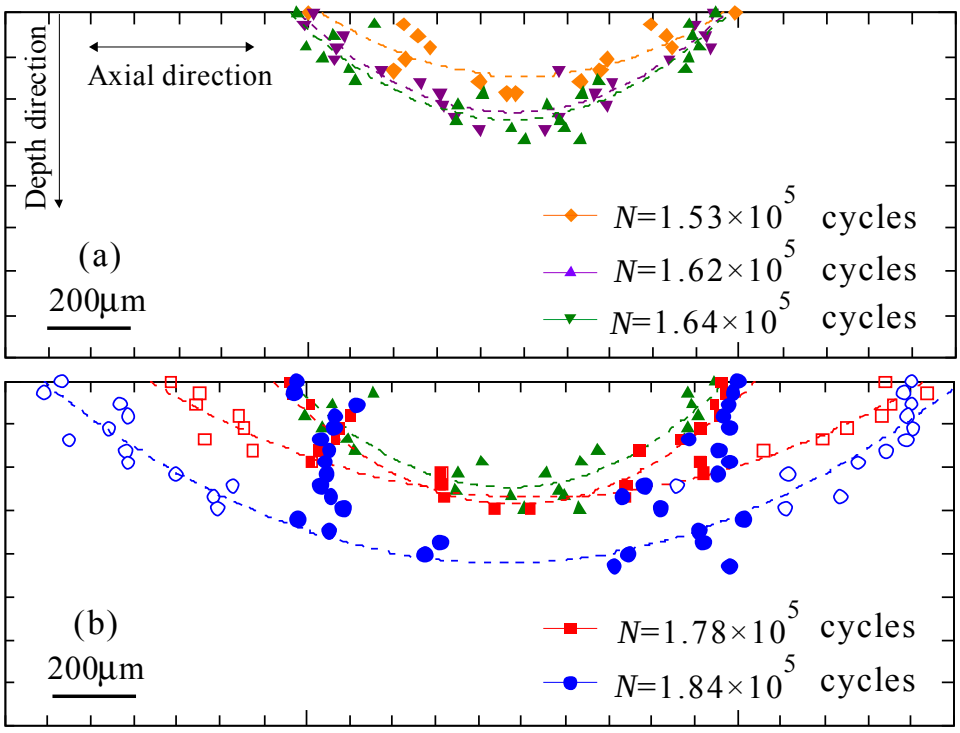

Figure 7. Internal shape of Crack A by measured by slices of μCT images.

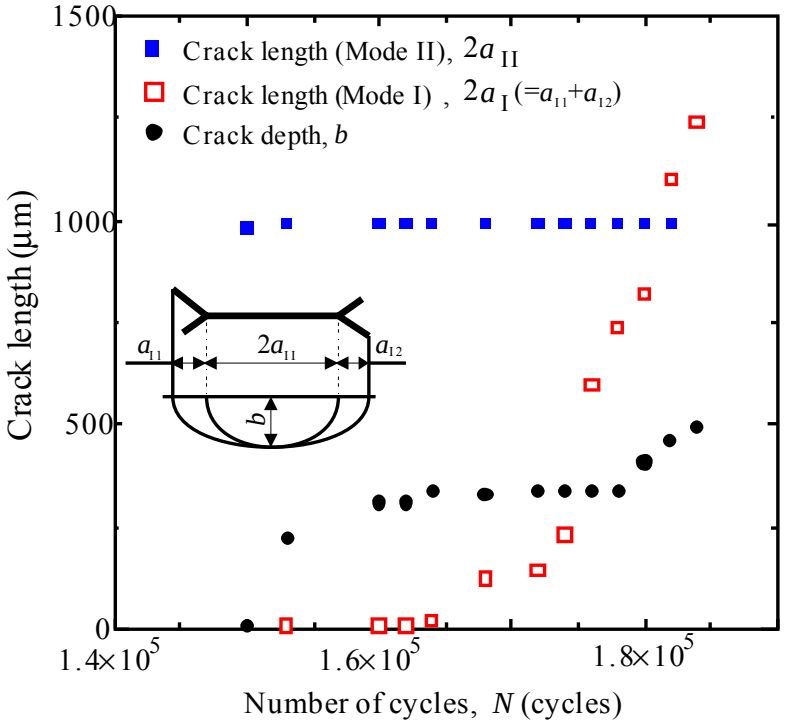

Figure 8. Crack growth curves of Crack A.

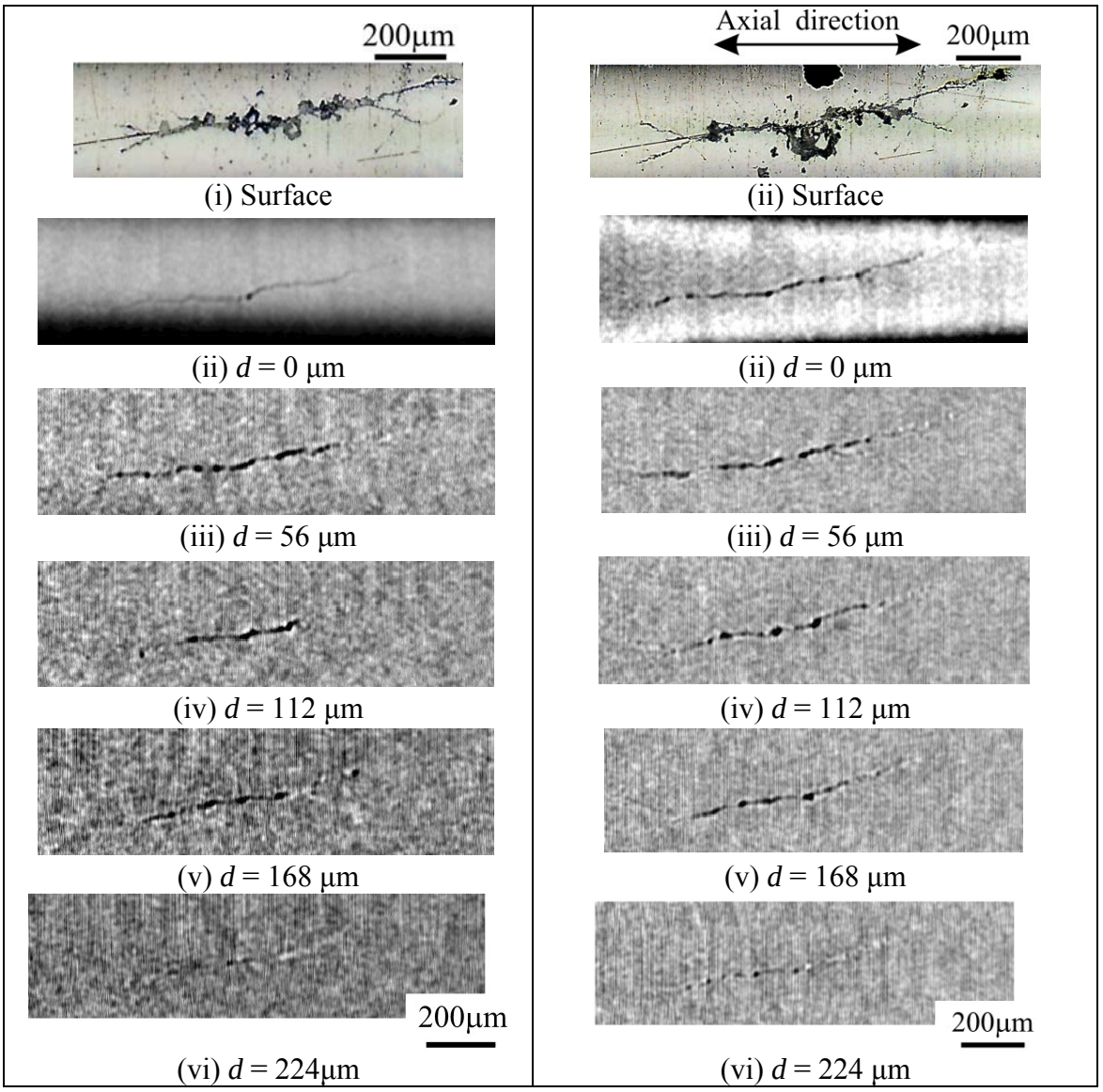

(a) N=1.05×10^5 cycles (b) N=1.11×10^5 cycles

Figure 9. CT image of Crack B under ta=435MPa.
((i) is obtained by optical microscope, (ii)~(vi) are obtained by CT)

reached to 320 μm. Then the branched crack grew at the surface without the growth in the depth direction. After the crack length at the surface reached to 175 μm (N=1.78×10^5 cycles), it grew both to the surface and to the depth directions.

Figure 8 shows the crack length as a function of number of cycles for the crack shown in Figure 7. The crack lengths at the surface, a_I and a_{II}, were measured both by an optical microscopy and CT imaging, those were almost consistent except at the very early stage of fatigue, while the crack depth, b, was measured only by the μCT imaging. The crack, however, was detected at the surface by optical microscope at N=9.30×10^4

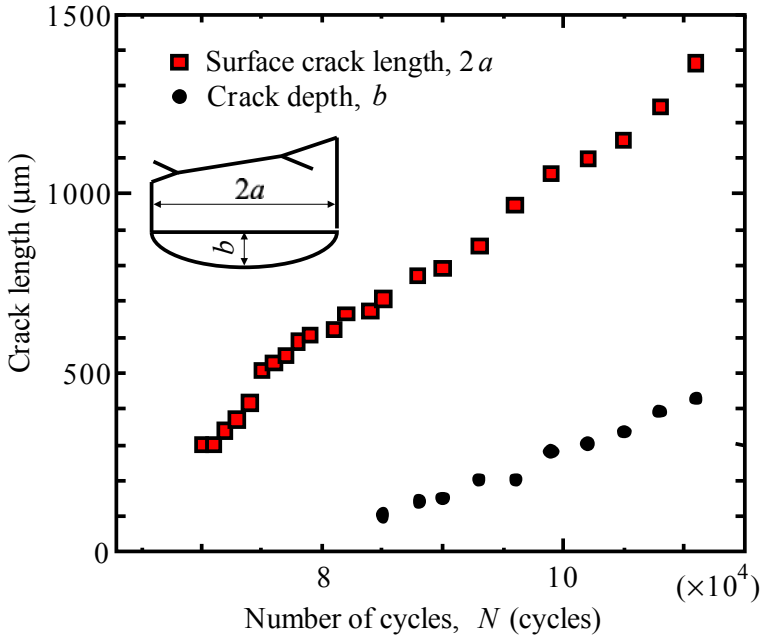

Figure 10. Crack growth curve of Crack B.

early stage of fatigue, while the crack depth, b, was measured only by the μCT imaging. The crack, however, was detected at the surface by optical microscope at N=9.30×10^4 cycles, while it could not be found by the μCT image, *i.e.*, the resolution of detector for CT imaging may responsible for this discrepancy. According to the theory of fracture mechanics, ideal shear mode cracks never open. For actual shear mode cracks, however, there are gap between crack faces because of the abrasion of crack faces. It may have reached to the critical size for the measurement of μCT at N=1.53×10^5 cycles.

Other examples of μCT images of a crack (Crack B) are shown in Figure 9, where the specimen was fatigued under the stress amplitude, τ_a, of 435 MPa and observed at N=1.05×10^5 and 1.11×10^5 cycles. In this case, the crack branched at the surface, but for the depth larger than 56 μm, the branching could not be observed. It means that the crack branching took place only in the surface layer. Then in most part of the crack, the change in the propagation mode from shear to tensile mode did not take place and the crack propagated dominantly by the shear mode.

Figure 10 shows the change of crack length as a function of number of cycles for Crack B. From N=7.2 ×10^4 to 8.5×10^4 cycles, the crack was observed at the surface by the optical microscope, but it could not be detected by the CT imaging like Crack A. The crack length at the surface increased with increasing the number of cycles. The crack depth could be measured after the abrasion powders were observed in the cracks as shown in Figure 9.

An example of a coalesced crack (Crack C) is presented in Figure 11, where the stress amplitude, τ_a, was 435 MPa. In the figure, solid marks and open marks indicate the sites of cracks tips before and after the branching, respectively. Two cracks

(a) Optical micrograph at N=9.90×10^4 cycles

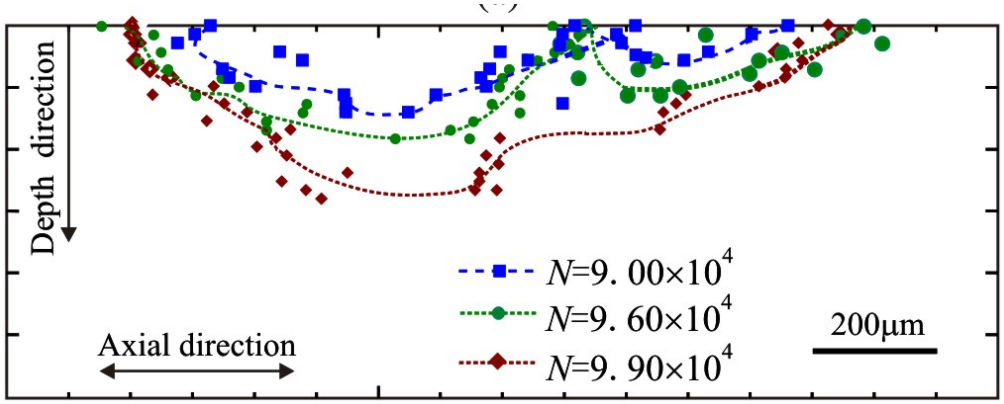

(b) Internal crack shape obtained by CT

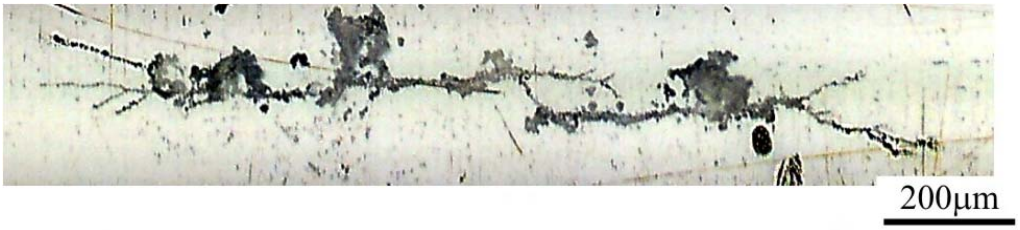

(c) Optical micrograph at N=1.11×10^5 cycle

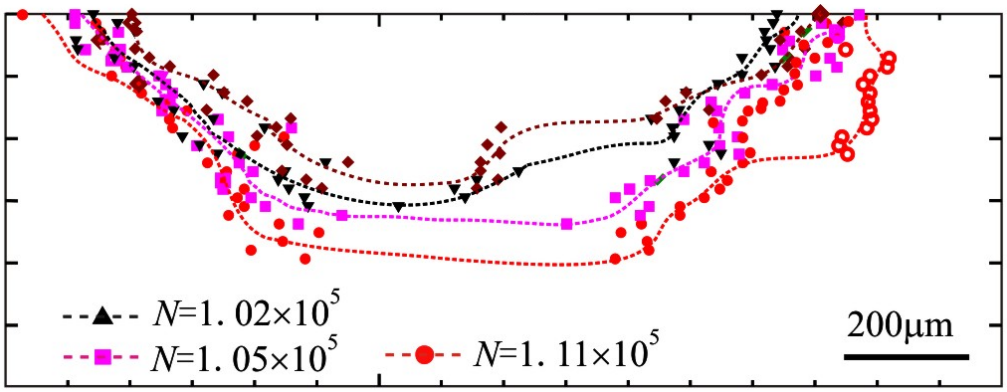

(d) Internal crack shape obtained by CT

Figure 11. Crack propagation behavior of Crack C from N=9.00×10^4 to 1.11×10^5 cycles.

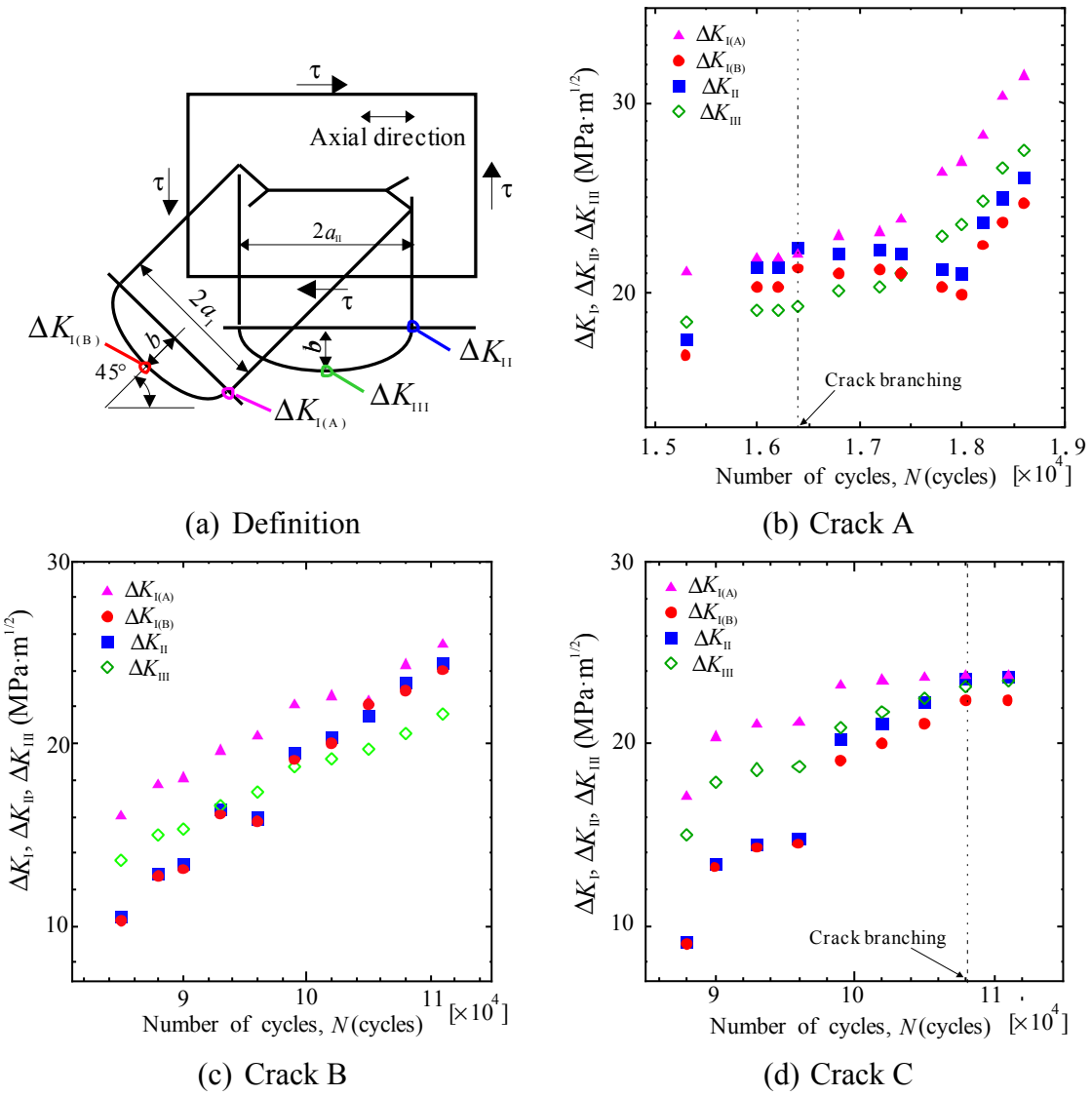

Figure 12. Change of stress intensity range.

coalesced at N=9.90×10^4 cycles. Figure 11 (b) indicates that the crack growth rate in the depth direction was very fast just before and after the coalescence. After the crack coalescence, the crack branching was observed both at and under the surface. The crack branching is considered to be triggered by the coalescence.

The stress intensity factor ranges, ΔK_{I}, ΔK_{II}, and ΔK_{III}, are plotted against the number of cycles in Figure 12, where $\Delta K_{\mathrm{I(A)}}$ and ΔK_{II} are the stress intensity factors at the crack tip at the surface, and $\Delta K_{\mathrm{I(B)}}$ and ΔK_{III} are the stress intensity factors at the depth of the crack tip. The stress intensity factor range, ΔK_{II} and ΔK_{III} were calculated by using Kaissir and Sih's equation [10] based on the crack shape projected to the plane parallel to the specimen axis. The values of $\Delta K_{\mathrm{I(A)}}$ and $\Delta K_{\mathrm{I(B)}}$ were calculated by using Irwin's equation [11],[12] based on the crack shape projected to the principal plane of stress, as

shown in Figure 12(a). The shear stress distribution was assumed to be constant in the depth direction for rough evaluation of the stress intensity factor. It is found from Figure 12(b) and (d) that $\Delta K_{I(a)}$ and ΔK_{II} of Crack A and C increased with increasing of the number of cycles, and reached 22~24MPa$\sqrt{m}$ when the crack branching were observed both at and under the surface. For Crack B, the crack branching was not been detected under the surface, and $\Delta K_{I(a)}$ and ΔK_{II} of Crack B were below 22~24MPa$\sqrt{m}$ for the observation period, as shown in Figure 12(c). From a comparison with the results, it can be concluded that the crack started to propagate in the tensile mode when ΔK_{II} at the crack tip at the surface reached 22~24MPa$\sqrt{m}$ and ΔK_{I} at the crack tip at the surface was over 22~24MPa$\sqrt{m}$.

Since the above discussion was based on the rough estimation of the stress intensity factor, calculation of the factor by the finite element analysys must be conducted for more precise analysis of the transition condition.

CONCLUSIONS

Micro computed tomography (SR-μCT) imaging using ultra-bright synchrotron radiation X-ray was applied to the observation of the torsion fatigue crack propagation behavior of a titanium alloy, Ti-6Al-4V. The results obtained are as follows.

(1) A compact torsion fatigue testing machine was developed to conduct fatigue test at Spring-8. The loading capacity of the machine was 5 Nm.
(2) The fatigue crack propagation behavior under reversed torsion was evaluated by the μCT technique. The crack propagation in the depth direction and propagation behavior of branched cracks and kinked cracks could be observed.
(3) The stress intensity factor ranges were calculated by considering the three-dimensional shapes of cracks. When the crack started to propagate in the tensile mode, ΔK_{II} at the crack tip on the surface reached 22~24MPa$\sqrt{m}$ and ΔK_{I} at the crack tip at the surface was larger than 22~24MPa$\sqrt{m}$.

ACKNOWLEDGEMENTS

The synchrotron radiation experiments were conducted at BL19B2 in SPring-8 with the approval of the Japan Synchrotron Radiation Research Institute (JASRI) under proposal numbers of 2008A1922 and 2009B1895. The authors are grateful for his technical support of Dr. Kentaro Kajiwara (JASRI).

REFERENCES

1. Murakami, Y., Takahashi, K. and Toyama, K. (2005) Fatigue Fract. Eng. Mat. Struct. **28**, 49-60.

2. Sawada, M., Bannai, K. and Sakane, M. (2005) J. Soc. Mat. Sci., Japan, **54**, 615-621.
3. Shiozawa, D., Nakai, Y., Morikage, Y., Tanaka, H., Okado, H. and Miyashita, T. (2006) Trans. Japanese Soc. Mech. Eng., Ser. A **72**, 1846-1852.
4. Shiozawa, D., Nakai, Y., Kurimura, T., Morikage, Y., Tanaka, H., Okado, H., Miyashita, T. and Kajiwara, K.(2007) J. Soc. Mat. Sci., Japan **56,** 951-957.
5. Nakai, Y., Shiozawa, D., Morikage, Y., Kurimura, T., Tanaka, H., Okado, H. and Miyashita, T. (2007) In: Fourth Int. Conf. on Very High Cycle Fatigue, pp. 67-72, Allison, J. E., Jones, J. W., Larsen, J. M. and Ritchie, R. O. (Ed.), TMS, Warendale, Pennsylvania.
6. Shiozawa, D., Nakai, Y., Kurimura, T. and Kajiwara, K. (2009) Proc. of 12th International Conference on Fracture, CD-ROM, OS12.086.
7. Nakai, Y. and Shiozawa, D. (2010) PJ Web of Conferences 6, 14th International Conference on Experimental Mechanics (ICEM 14), 35004.
8. Matsunaga, H., Muramoto, S, Shomura, N. and Endo, M. (2009) J. Soc. Mat. Sci., Japan, **58**, 773-780.
9. Campbell, J.P. and Ritchie, R.O. (2000) Eng. Fract. Mech. **67**, 229-249.
10. Kassir, M.K. and Sih, G.C. (1966) J. App. Mech., **33**, 601-611.
11. Irwin, G.R. (1962) Trans. ASME Ser E: J. Appl. Mech. **29**, 651-654.
12. Murakami, Y. (1987) *Stress Intensity factors Handbook* **2**, pp. 696-689, Soc. Mat. Sci, Japan, Kyoto.